

Effect of Pu content on uncertainty in reactor parameters due to use of no temperature gradient in (U-Pu)O₂ fuels

Mehmet TÜRKMEN*

Department of Nuclear Engineering, Faculty of Engineering, Hacettepe University, Ankara, Turkey

Received: 20.09.2016

Accepted/Published Online: 07.02.2017

Final Version: 18.04.2017

Abstract: Radial temperature distribution in a fuel rod is a parabolic function. Neutronics calculations are in general performed over a volume-averaged temperature by ignoring this distribution. Such an assumption results in an uncertainty in reactor design parameters. In this study, the magnitude of this uncertainty is estimated by solving the heat equation with a temperature-dependent conductivity coefficient coupled with a reactor physics code. The effect of radial fuel temperature distribution is investigated by representing the fuel region as multiregional. Uncertainty is investigated for various Pu contents of (U-Pu)O₂ fuel, a mix of depleted U and reactor-grade Pu. The effect of Pu content on the uncertainty is studied. The PWR TMI-1 unit cell case from UAM test problems is used in the calculations. Results are obtained by using the discrete ordinate method. From the results, it was observed that uncertainties in reactor parameters (k_{∞} and Doppler coefficient) due to the use of no temperature gradient and in k_{∞} due to cross-sections decrease as Pu content increases. Moreover, it was calculated that uncertainty due to uniform temperature inside the nuclear fuel is about 7% of uncertainty due to cross-sections.

Key words: (U-Pu)O₂ fuel, SCALE6, uncertainty analysis, temperature gradient, Doppler feedback, cross-section

1. Introduction

Estimation of various uncertainty sources such as those due to experimental data and approximations and assumptions in modeling is important in reactor design for accurate neutronics calculations. Among the uncertainties, uncertainty in the infinite multiplication factor (k_{∞}) due to omitting the spacer grid in modeling was investigated by Tran and Cho [1]. When the spacer grid was replaced with H₂O in modeling, k_{∞} was calculated higher due to more neutron moderation and the effect of the spacer grid on k_{∞} was found to be 400 pcm. The impact of atom density on uncertainty of the effective multiplication factor k_{eff} due to nuclear data uncertainties was also investigated in a different study [2] and it was reported that uncertainty increases as atom density increases.

In addition to uncertainty in modeling, fuel type is also a significant factor on uncertainty. For instance, uncertainty analyses were carried out for U fuels in a research project [3]. It was found in that work that there is an underestimation of 60–100 pcm in k_{∞} for U fuel. The capability of reactor physics codes and nuclear data libraries for the systems loaded with U-Pu fuel, which forms the subject of this study, and the accuracy of predictions for various core configurations loaded with U-Pu and U fuels were investigated in the KRITZ experiments [4]. k_{eff} results obtained by using reactor physics codes for U-Pu fuels agree with experiments

*Correspondence: tm@hacettepe.edu.tr

by showing deviations of $\sim 0.16\%$ at room temperature and $\sim 0.18\%$ at elevated temperature. Uncertainty and sensitivity analysis of KRITZ-2 experiments are most sensitive to the fission cross-section of the Pu-239 isotope and capture cross-section of the U-238 isotope. Uncertainty is less sensitive to the capture cross-section of the U-238 isotope compared to U fueled systems.

On the other hand, U-Pu fuel has different neutronic, physical, and chemical properties due to Pu content than U fuel. This causes a new set of changes in existing reactor designs designed to burn U fuels in order to burn U-Pu fuels. The most important is reevaluation of reactor safety criteria for U-Pu fuel. The greater neutron absorption cross-section of Pu than U causes use of lower burnable poison and need for less control rod worth. Furthermore, fissile Pu isotopes produce more energy per fission. However, the thermal conductivity coefficient of U-Pu fuel is 10% less than that of U [5].

In the case of the Doppler coefficient of reactivity, U-Pu fuel provides more negative values than U fuel [6]. In addition, there is no generally accepted value for U-Pu fuel, although the uncertainty of the Doppler coefficient of the U fuel used in reactor safety calculations is assumed to be 10% [7]. For the reasons stated above, it may be expected that the U-Pu fuel has higher uncertainty in k_∞ , Doppler coefficient, and reaction rate.

Another important source of uncertainty is the use of no temperature gradient (so-called uniform temperature or isothermal approach) in nuclear fuel, which is also under investigation in this study. Despite the fact that a radial temperature profile has a parabolic distribution, a volume-averaged uniform temperature is used in most neutronics calculations. In this study, the magnitude of this uncertainty is estimated by solving the heat equation with a temperature-dependent conductivity coefficient coupled with a reactor physics code.

2. Modeling and method for uncertainty calculation

2.1. Problem definition

Calculations are carried out by using the PWR TMI-1 unit cell case introduced in the UAM test problems [8]. Unit cell modeling, the smallest representation of reactor core, is used in analyses. Material and geometric properties of the unit cell are tabulated in Table 1. The multiregion model in square lattice geometry is shown in Figure 1.

As seen in Figure 1, the fuel region is defined as multiregional, with small regions of equal volumes. In the study, the fuel region is divided into 18 regions at most, to the extent permitted by the used deterministic code. In the calculations, fuel surface temperature and average fuel temperature over whole regions are kept constant and are set to 600 and 900 K, respectively.

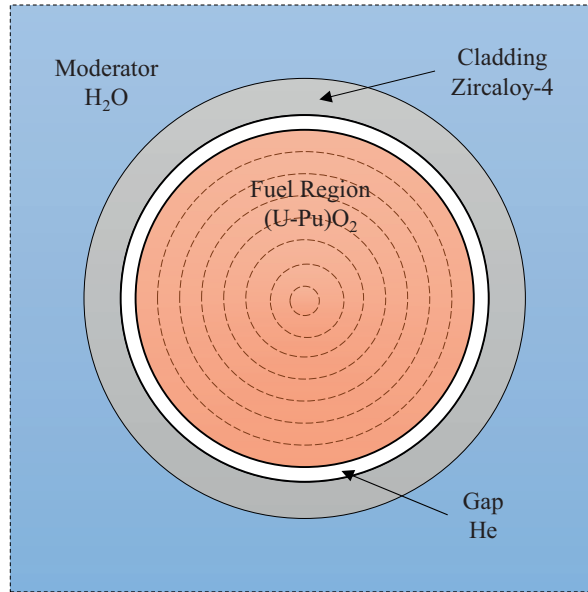
(U-Pu)O₂ MOX (Mixed OXide) fuels are formed by mixing depleted U (DU) with reactor-grade Pu (RG-Pu) in various fractions. Pu content, y , in (U_{1-y}Pu_y)O₂ fuel is changed between 0.08 and 0.66. Isotopic compositions of RG-Pu and DU are from a study of Doppler defect [7] and are tabulated in Table 2.

Deterministic results are obtained by using SCALE6.0 TSUNAMI-1D [9,10] with the S_n method. The 238-group ENDF/B-VII (v7-238) is used in TSUNAMI-1D calculations. SCALE is a comprehensive modeling and simulation package for nuclear safety analysis and design in nuclear installations and transport/storage designs. The code can handle reactor physics, criticality safety, radiation shielding, radioactive source characterization, fuel depletion, and sensitivity and uncertainty analyses. It offers 89 “plug and play” computation modules with 3 deterministic and 3 Monte Carlo radiation transport solvers that can be selected depending on the desired solution strategy.

In the code, the default module (BONAMIST) which is suggested for ENDF/B-V and later is used

Table 1. PWR TMI-1 unit cell parameters.

Parameter	Unit	Value
Pitch	mm	14.427
Fuel pellet diameter	mm	9.391
Fuel pellet material		$(U_{1-y}Pu_y)O_2$
Fuel density	g/cm^3	Eqs. (6) & (7a/b)
Fissile content	wt. %	4.85-24
Clad outside diameter	mm	10.928
Clad thickness	mm	0.673
Clad material		Zircaloy-4
Clad material density	g/cm^3	6.55
Gap material		He
Moderator/coolant material		H ₂ O
Hot full power condition		
Volume-averaged fuel temperature	K	900.0
Clad temperature	K	600.0
Moderator/coolant temperature	K	562.0
Moderator/coolant density	kg/m^3	748.4

**Figure 1.** Multiregion representation of PWR TMI-1 fuel pin unit-cell (unscaled).**Table 2.** Isotopic content of reactor-grade Pu and depleted U.

Isotope	RG-Pu (at. %)	Isotope	DU (wt. %)
Pu-239	45.0	U-234	0.002
Pu-240	30.0	U-235	0.250
Pu-241	15.0	U-238	99.748
Pu-242	10.0		

for cross-section processing. For cylindrical geometry, inner and outer boundaries are “reflected” at the fuel centerline and “white” boundary condition at the rod surface, respectively. MULTIREGION is selected for the

resonance self-shielding model. In this approach, the lattice geometry effects are not included in the generated cross-sections. In the CENTRM module, the maximum number of inner iterations for each outer iteration in CENTRM, maximum number of outer iterations in the thermal range, and integral/point-wise convergence criteria were changed to 40, 6, and 1e-8, respectively. The rest are at default values. In the XSDRNPM module, angular quadrature sets, outer iterations, inner iterations, and the convergence criterion on the outer iteration and the point flux were increased to 32, 100, 40, and 1e-8, respectively. The spatial mesh factor was selected to be 0.2 by a five-times increment. A default covariance data file, the 44GROUPV5COV covariance matrix, was used in SAMS calculations. Implicit sensitivity calculation was enabled.

Distribution of volumetric heat generation rate (radial power profile) was obtained by using the converged region-wise fission source values given in the TSUNAMI-1D output file.

Heat deposition in fuel due to gamma heating is neglected in this study as the deposition has a homogeneous distribution inside the fresh fuel and has no effect on the distribution of the heat generation rate.

Doppler feedback of reactivity (α) is obtained by using Eq. (1). HZP and HFP cases mean hot zero power and hot full power, respectively. The only difference between the cases is that fuel temperature is at 600 K in HZP.

$$\alpha_{DC} = \frac{\Delta\rho}{\Delta T} = \frac{\rho_{HZP} - \rho_{HFP}}{T_{HZP}^F - T_{HFP}^F} \quad (1)$$

Here, T is the temperature of the fuel region (with superscript F) and ρ is the reactivity of the system.

Axial temperate gradient effect is not within the scope of this study.

2.2. Calculation of uncertainty

Radial temperature distribution in a fuel pin can be found by numerically or analytically solving the heat equation (Eq. (2)) for a temperature-dependent thermal conductivity coefficient and space-dependent volumetric heat generation rate at steady-state condition in a cylindrical coordinate system.

$$\frac{1}{r} \frac{\partial}{\partial r} \left(k(\vec{r}, T) r \frac{\partial T(\vec{r})}{\partial r} \right) + \dot{q}(\vec{r}) = 0 \quad (2)$$

Here, r is the radius, T is the temperature, k is the thermal conductivity, and \dot{q} is the volumetric heat generation rate.

In Eq. (2), the thermal conductivity coefficient depends on the material composition and temperature of the fuel. \dot{q} is a function of radius and in direct proportion to the fission reaction rate. The solution of Eq. (2) becomes Eq. (3) for constant volumetric heat generation rate and single volume fuel.

$$\int_{T_o}^{T_i} k(T) dT = \bar{q} (R_o^2 - R_i^2) / 4 \quad (3)$$

Here, T_i and T_o are the inner and outer surface temperatures, respectively, and \bar{q} is heat generation rate averaged over the region bounded by R_o and R_i .

For a fuel pellet split into n equal volumes, Eq. (3) can be expressed as follows.

$$\sum_{j=1}^n \left[\int_{T_o^j}^{T_i^j} k_j(T) dT \right] = \sum_{j=1}^n \left[\bar{q}_j (R_{o_j}^2 - R_{i_j}^2) / 4 \right] \quad (4)$$

With known T_o , R_o , and R_i , T_i can be calculated from the conductivity integral by integrating k between T_o and T_i . Inner and outer surface temperatures of each fuel region can readily be obtained. Using this profile, the volume-averaged temperature of each region can be calculated.

The (U-Pu)O₂ thermal conductivity to be used in Eq. (4) is given in Eq. (5). This equation is valid in the range of $700 \leq T \leq 3100$ K and $3\% \leq \text{Pu} / (\text{Pu}+\text{U}) \leq 15\%$ for 100% theoretical density (ρ_{TD}), and it contains 7% uncertainty due to the goodness of fit and distribution of the experimental data [11].

$$k(T, x) = k_0(T, x) \times FM \quad (\text{W/m-K}) \quad (5)$$

Here, $k_0(T, x) = \frac{1.1579}{A+CT} + 2.3434 \times 10^{11} \times T^{-5/2} \times e^{-16350/T}$ (W/mK) and porosity effect $FM = (1-p)/(1+2p)$ for porosity $p = (\rho_{TD} - \rho)/\rho_{TD}$.

Here, $A(x) = 2.85x + 0.035$ (mK/W) and $C(x) = (-7.15x + 2.86) \times 10^{-4}$ (m/W). $x (= 2 - \text{O/M})$, deviation from the stoichiometry, is 0 for an O/M ratio of 2. Radiation effect is not included in the calculations.

As seen from Eq. (5), the thermal conductivity of (U-Pu)O₂ fuel changes with composition, density, and stoichiometry.

The U-Pu fuel density is higher than that of U fuel, increasing as Pu content increases and decreasing as temperature increases. Solid (U_{1-y}Pu_y)O₂ fuel density has a linear relationship with Pu content (y) for $0 \leq y \leq 1$. The relation is shown in Eq. (6) [11].

$$\rho(273K) = 10.970 + 0.490y \quad (\text{g/cm}^3) \quad (6)$$

Change of density with temperature is given below for the range of $273 < T < 973$ K.

$$\rho(T) = \rho(273K) \times (9.9734 \times 10^{-1} + 9.802 \times 10^{-6}T - 2.705 \times 10^{-10}T^2 + 4.391 \times 10^{-13} \times T^3)^{-3} \quad (7a)$$

For 973 K and over:

$$\rho(T) = \rho(273K) \times (9.9672 \times 10^{-1} + 1.179 \times 10^{-5}T - 2.429 \times 10^{-9}T^2 + 1.219 \times 10^{-12} \times T^3)^{-3} \quad (7b)$$

A single volume fuel region is used in calculations as a reference case to understand the effect of the use of no temperature gradient. Starting from a single volume, fuel was divided into 2, 4, 8, 12, 14, 16, and 18 regions. In the first stage of the calculation, it was assumed that the volumetric heat generation rate of each region is equal and is assumed to be 1 as an initial guess. The inner surface temperature (T_i) of each region can be calculated from Eq. (3) once the initial volumetric heat generation rate and Eq. (5) are inserted into Eq. (3). The calculated temperature distribution, $T_i(r)$, is fit to a fourth-order polynomial equation with an accuracy of R^2 (goodness of fit) > 0.99 and used to calculate the volume-averaged temperature of each fuel region. It is important to mention here that the volume-averaged temperature over all the regions equals the value (900 K) used in the isothermal approximation. By this means, it is possible to accurately estimate the effects of radial temperature distribution. The calculated temperature of each region is supplied as input to the reactor physics code. The code produces output containing the fission source distribution caused by the supplied volume-averaged temperatures. This calculated new fission source distribution is replaced with the old one so as to make a new iteration. This process is repeated until the fission source distribution converges to a predetermined convergence criterion. Once the fission source distribution is converged, calculations are repeated for the next multiregion case. This process proceeds until the temperature gradient effects are completely modeled. A computational flow diagram is given in Figure 2. The main steps are outlined below.

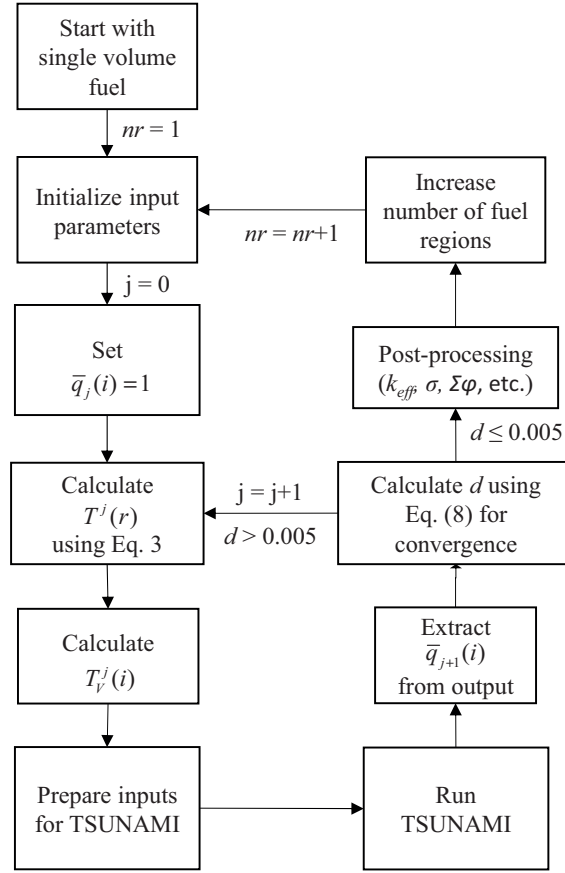


Figure 2. Computational flow diagram.

- Start calculations for single volume fuel region ($nr = 1$).
- For iteration $j = 0$, set volume heat generation rate $[\bar{q}_j(i) = 1]$ to 1 for region i with a total region size of n .
- Evaluate the temperature distribution $T^j(r)$ by using Eq. (3).
- Using $T^j(r)$, calculate the volume-averaged temperature $[T_V^j(i)]$ of each region.
- Prepare the input file for the reactor physics code by using the calculated T_V^j .
- Run the code and obtain a new heat generation rate $\bar{q}_{j+1}(i)$ for each region from the fission source distribution.
- Calculate the Euclidian distance using the following formula:

$$d = \sqrt{\sum_{i=1}^{nr} |\bar{q}_j(i) - \bar{q}_{j-1}(i)|^2} \quad (8)$$

- If $d < 0.005$, stop searching and go to the postprocessing step.

- Increase the number of fuel regions by one ($nr = nr + 1$). Then go to the second step for the initiation of the iteration.
- If not, proceed with the iteration by increasing the iteration number ($j = j + 1$), calculate the new $T^{j+1}(r)$ by using $\bar{q}_{j+1}(i)$, and then go to the input preparation step.

The convergence criterion, d , performed by Euclidean distance, which measures the distance between two n-dimensional points, is selected to less than 0.005. The reason for the use of Euclidean distance is that at least two digits after the decimal point for the volumetric heat generation rate of each region are desired to converge.

3. Results

The change of thermal conductivity (W/mK) and density of PuO_2 and UO_2 fuels with temperature is illustrated in Figure 3. As seen, the thermal conductivity of Pu is higher than that of U. This difference increases as the temperature increases. Thermal conductivity changes from 5 to 2 W/mK in the range of $600 \leq T \leq 1300$ K. Furthermore, the density of Pu is greater than that of U, but the difference remains almost constant with increasing temperature. It was shown in different studies [12] that the addition of Pu into the U matrix reduces thermal conductivity and density. These variations would result in a change in space-dependent reaction rates and thus in temperature profile.

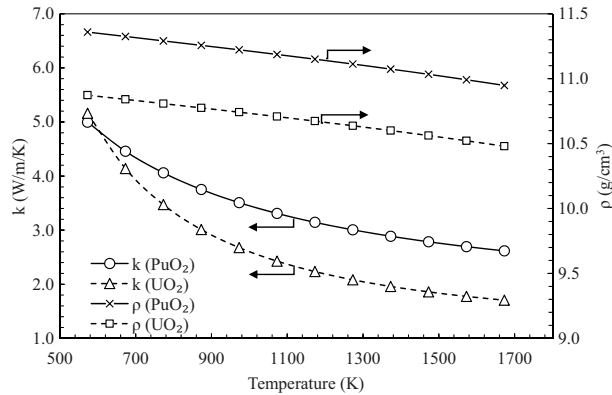


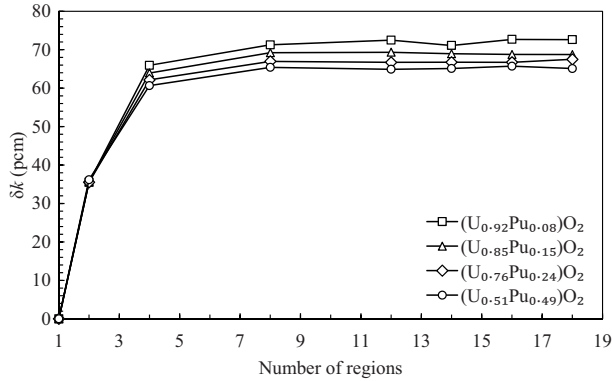
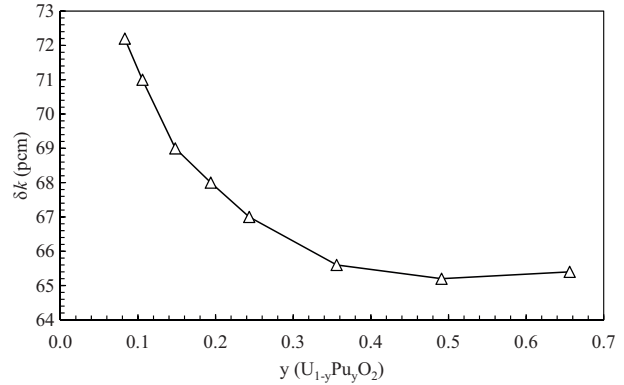
Figure 3. Change of density and thermal conductivity of UO_2 and PuO_2 fuels with temperature.

Effect of uniform temperature on the infinite core multiplication factor (k_∞) for various Pu contents is given in Table 3. Variation of uncertainty ($\delta k = k_\infty^{T(r)} - k_\infty^{900}$) in k_∞ with number of regions in units of pcm (10^{-5}) is presented in Figure 4 for various Pu contents.

As seen from the k_∞^{900} column, even if the criticality problem is modeled without a temperature gradient, multiregional representation of the fuel has a significant effect on the SCALE6 results due to self-shielding effect. From Figure 4, as the number of regions increases, uncertainty due to the isothermal approach first quickly increases and then levels off after 4 regions. The leveled-off values change with Pu content. Uncertainty decreases as Pu content goes up. This reduction is more clearly seen in Figure 5. These values are convergent values and are the mean values calculated using the results of the last four multiregions. It was observed from the results that uncertainty decreases starting from about 72 pcm and approaches about 65 pcm after about 50% Pu (0.5 y).

Table 3. Change of k_{∞} with number of regions for various Pu content.

	$k_{\infty}^{T(r)}$			k_{∞}^{900}		
	y = 0.08	y = 0.24	y = 0.49	y = 0.08	y = 0.24	y = 0.49
1	1.14489	1.26205	1.38930	1.14489	1.26205	1.38930
2	1.14508	1.26241	1.38981	1.14473	1.26205	1.38945
4	1.14560	1.26294	1.39038	1.14494	1.26232	1.38978
8	1.14592	1.26325	1.39069	1.14520	1.26258	1.39004
12	1.14606	1.26336	1.39078	1.14533	1.26269	1.39014
14	1.14608	1.26340	1.39081	1.14537	1.26273	1.39016
16	1.14613	1.26342	1.39085	1.14540	1.26276	1.39019
18	1.14615	1.26345	1.39086	1.14542	1.26278	1.39021

**Figure 4.** Change of uncertainty (δk) in k_{∞} with number of regions for various Pu contents.**Figure 5.** Change of uncertainty (δk) in k_{∞} due to isothermal approach with Pu content.

Calculated power profiles for various Pu contents in 18-region calculation are illustrated in Figure 6. Change in radial power peaking factor shows a parabolic distribution due to self-shielding, temperature effect, and flux depression. Moreover, the distribution significantly varies depending on Pu content. As the Pu fraction in U-Pu fuel increases, the amount of heat produced in the region near the fuel surface increases and the difference in heat generation between the surface and center increases. The main reason for this is that an increase in Pu content in fuel leads to an increase in the amount of fissile Pu isotopes, and thus in fission rate, near the fuel surface.

Change of temperature with radius for various Pu contents in 18-region calculation is depicted in Figure 7. As seen from Figure 7, the centerline temperature decreases as Pu content increases. Centerline temperatures for 0.08 y and 0.49 y are 1200 K and 1170 K, respectively. This situation, as seen from Figure 6, can be described by a lower heat generation rate at the center. Similarly, a higher power peaking factor causes a higher temperature near the fuel surface.

Change of the Doppler coefficient of reactivity with number of regions for various Pu contents is depicted in Figure 8. As the number of regions increases, the Doppler coefficient calculated by using temperature distribution increases before 4 regions and then becomes stable. In the case of the use of no temperature gradient, there is no change in the coefficients. A lower Doppler coefficient is calculated in the isothermal case compared to temperature distribution. Deviation from the isothermal case also decreases as Pu content increases. The deviation from the isothermal case and the Doppler coefficient with Pu content is more clearly shown in Figure 9. These values are convergent values and are the mean values calculated using the results of the last four multiregions. From the results, the Doppler coefficient linearly increases from -3 to -2 pcm/K

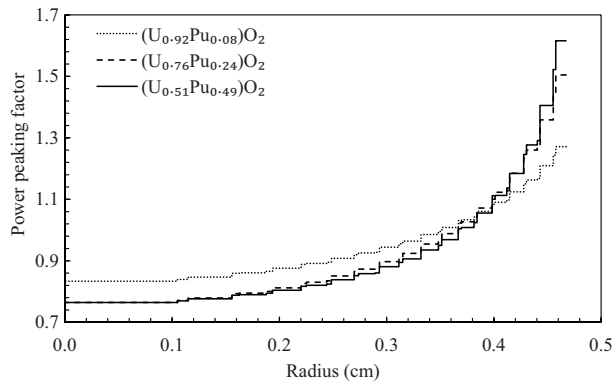


Figure 6. Calculated radial power profiles for various Pu contents.

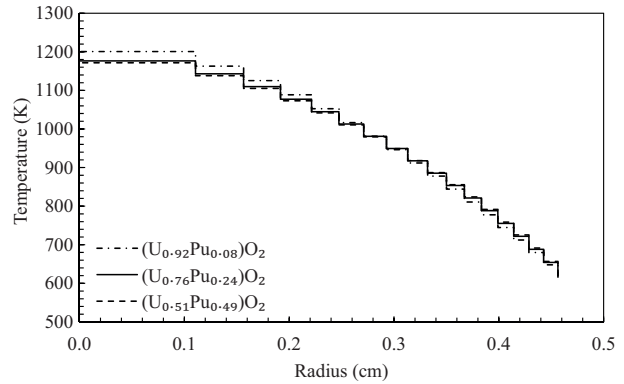


Figure 7. Temperature distribution for various Pu contents.

as Pu content increases. Moreover, deviation from the isothermal case decreases exponentially and approaches about 4.80%.

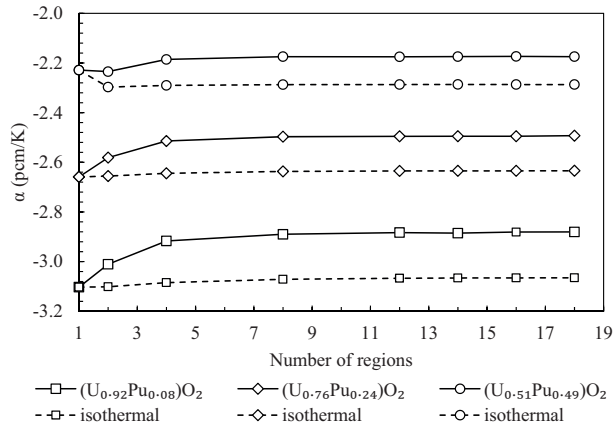


Figure 8. Change of Doppler coefficient with number of regions for various Pu contents.

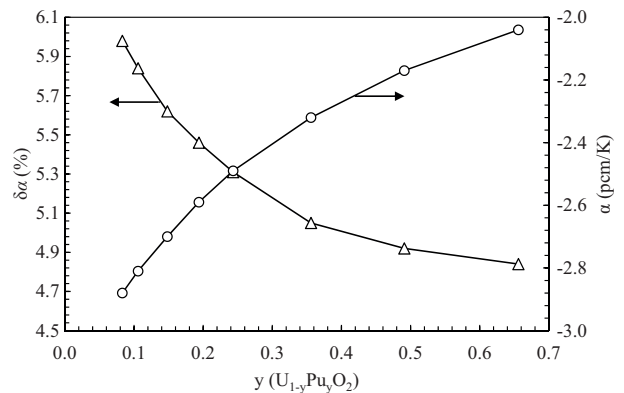


Figure 9. Change of deviation from the isothermal case and Doppler coefficient with Pu content.

Change of uncertainty ($\% \delta k/k$) due to cross-sections with number of regions for various Pu contents is depicted in Figure 10. Uncertainty values calculated by using temperature distribution are the same values as in the isothermal case; therefore, only results of temperature distribution are given in Figure 10. From the results, uncertainty does not vary with the number of regions but rather varies with Pu content. Change of $\% \delta k/k$ and δk (pcm) uncertainties due to cross-sections with Pu content is presented in Figure 11. Uncertainty in terms of δk slightly decreases to 0.15 y from 0.08 y and then increases in a linear way. However, fraction in k_{∞} ($\% \delta k/k$) decreases as Pu content increases. The uncertainties in Pu contents of 0.08 and 0.66 are calculated to be 0.84% (960 pcm) and 0.70% (1020 pcm), respectively.

4. Discussion

In this study, the uncertainty in reactor parameters due to the use of no temperature gradient was examined for various Pu fractions of U-Pu fuel. Results of calculations show that the power profile in the radial direction is significantly affected by the Pu content of the fuel. An increase in Pu content results in an increase in k_{∞} , higher power peaking near fuel surface, lower centerline temperature, and a less negative Doppler coefficient.

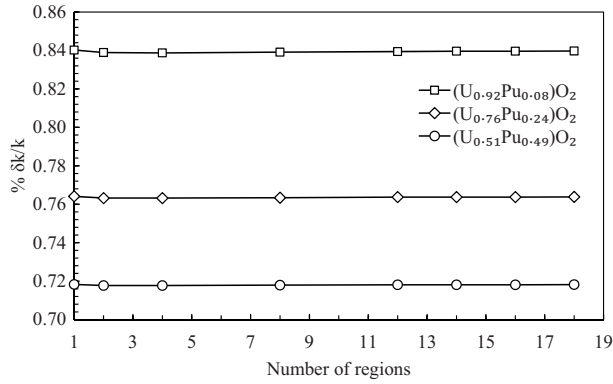


Figure 10. Change of uncertainty ($\% \delta k/k$) due to cross-sections with number of regions for various Pu contents.

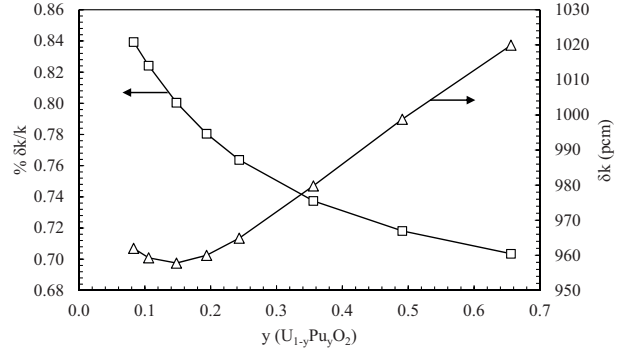


Figure 11. Change of uncertainty ($\% \delta k/k$) due to cross-sections with Pu content.

Uncertainty in k_∞ due to use of the isothermal approach for 4.85% enriched UO_2 fuel was reported as 100 ± 8 pcm for MCNP6 [13] and 60 pcm for SCALE6 [3]. In the case of 4.85% fissile content of RG-MOX (reactor-grade MOX) and WG-MOX (weapons-grade MOX) fuel, uncertainties calculated by using MCNP6 were found to be 100 ± 9 and 90 ± 9 pcm, respectively [14]. In this study, uncertainty calculated by using SCALE6 for fuel ($\text{U}_{0.92}\text{Pu}_{0.08}\text{O}_2$) having the same enrichment with 4.85% UO_2 is 72 pcm. This implies that the magnitude of uncertainty depends on the reactor physics code used. However, it can also be said that the order of uncertainty is the same for the same fissile content.

The Doppler coefficient varies between -3 and -2 pcm/K depending on Pu content. A Doppler coefficient of -2.88 pcm/K was obtained for 0.08 y, whereas it is -1.62 ± 0.02 pcm/K for the same fissile content of U fuel [3]. In this respect, U-Pu fuels have less negative Doppler coefficients than U fuels. On the other hand, it was demonstrated in a study on U-Pu fuels [14] that uncertainty in Doppler coefficients of U-Pu fuels is lower than that of U fuel. In addition to this, uncertainties in Doppler coefficients of 4.85% WG-MOX and 4.85% RG-MOX fuels calculated by using MCNP6 were reported to be 7% and 8%, respectively [14]. In this study, uncertainty in Doppler coefficient of 4.85% RG-MOX fuel calculated by using SCALE6 was about 6%. Uncertainty in Doppler coefficients of U fuels of 10% is already accepted and used in reactor safety calculations [7]. In spite of lower uncertainty in U-Pu fuel than U fuel, for more conservative calculations, the uncertainty used in U fuel can be used in U-Pu fuel, as well. However, it is clear that the use of 6% uncertainty in safety calculations has advantages during operation from the viewpoint of reactor economy.

For 0.08 y to 0.49 y Pu content, uncertainty in k_∞ due to the isothermal approach is in the range of 72 to 65 pcm, whereas uncertainty in the Doppler coefficient due to the isothermal approach is in the range of 6% to 4.8%. Uncertainty (δk) in k_∞ due to cross-sections is in the range of 962 to 1020 pcm. Therefore, total uncertainty is in the range of 1034 to 1085 pcm. Total uncertainty for 4.85% enriched U fuel was reported to be 752 (60 + 692) pcm [3]. This shows that uncertainty in U fuel is lower than that in U-Pu fuel. Similarly, U-Pu fuels have higher uncertainty in Doppler coefficients. In addition, uncertainty in U-Pu fuels due to cross-sections is higher than that in U fuels considering uncertainty of 0.49% (700 pcm) in 4.85% U fuel [3].

It was calculated that uncertainty in k_∞ due to no temperature gradient is about 7% of uncertainty due to cross-sections. This value was found to be 10% in U fuel. In this respect, uncertainty due to cross-sections within total uncertainty plays a more important role in determining reactor safety criteria.

Besides uncertainties due to no temperature gradient and cross-sections, other uncertainty sources such as

rod-to-rod variation of fuel/clad/moderator/coolant/gap material atom density, spacer-grid effect in modeling, and variations in material sizes during fabrication need to be specified and calculated.

In summary, it was found from the results that uncertainties in k_{∞} and the Doppler coefficient of reactivity and uncertainty ($\% \delta k/k$) in k_{∞} due to cross-sections decrease as the Pu content of the fuel increases. On the contrary, it was observed that uncertainty (δk) in k_{∞} due to cross-sections increases.

Acknowledgments

This study was supported by a grant from the Scientific and Technological Research Council of Turkey (TÜBİTAK-1001-114F375).

References

- [1] Tran, X. B.; Cho, N. Z. *Nucl. Eng. Technol.* **2016**, 48, 33-42.
- [2] Kaddour, M.; El Bardouni, T.; Boulaich, Y.; Allaoui, O.; El Bakkari, B.; El Younoussi, C.; Azahra, M.; Boukhal, H.; EL Ouahdani, S.; Chakir, E. *Int. J. Innov. Appl. Stud.* **2013**, 4, 171-181.
- [3] Sökmen, C. N.; Türkmen, M.; Çelikten, O. S.; Konur, G.; Sarıcı, G.; Beydoğan, N. *Nükleer Yakıt Elemanı Tesir Kesitlerine Radyal Sıcaklık Dağılımlarının Etkisinin İncelenmesi. TÜBİTAK Proje No: 1001-114F375*; TÜBİTAK: Ankara, Turkey, 2016 (in Turkish).
- [4] NEA. *Benchmark on the KRITZ-2 LEU and MOX Critical Experiments. Final Report, NEA/NSC/DOC(2005)24*; OECD: Paris, France, 2005.
- [5] Topliss, J. R.; Palmer, I. D.; Abeta, S.; Irida, Y.; Yamate, K. *Measurement and Analysis of MOX Physical Properties. IAEA-TECDOC-941*; International Atomic Energy Agency: Vienna, Austria, 1997.
- [6] Conlin, J. L. In *Joint International Topical Meeting on Mathematics & Computation and Supercomputing in Nuclear Applications*, Monterey, CA, USA, 15–19 April 2007; American Nuclear Society: LaGrange Park, IL, USA, 2007, CD-ROM.
- [7] Mosteller, R. D. In *Joint International Topical Meeting on Mathematics & Computation and Supercomputing in Nuclear Applications*, Monterey, CA, USA, 15–19 April 2007; American Nuclear Society: LaGrange Park, IL, USA, 2007, CD-ROM.
- [8] Ivanov, K.; Avramova, M.; Kodeli, I.; Sartori, E. *Benchmark for Uncertainty Analysis in Modelling (UAM) for Design, Operation and Safety Analysis of LWRs, Volume I: Specification and Support Data for the Neutronics Cases (Phase I)*; NEA/OECD Nuclear Energy Agency: Paris, France, 2007.
- [9] ORNL. *SCALE: A Modular Code System for Performing Standardized Computer Analyses for Licensing Evaluation, ORNL/TM-2005/39, Version 6, Vols. I-III*; Oak Ridge National Laboratory: Oak Ridge, TN, USA, 2009.
- [10] Rearden, B. T. *TSUNAMI-1D: Control Module for One-Dimensional Cross-Section Sensitivity and Uncertainty Analysis for Criticality, ORNL/TM-2005/39, Version 6, Vol. I, Sect. C8*; Office of Nuclear Material Safety and Safeguards, U.S. Nuclear Regulatory Commission: Washington, DC, USA, 2005.
- [11] Popov S. G.; Carbajo, J. J.; Ivanov, V. K.; Yoder, G. L. *Thermophysical Properties of MOX and UO₂ Fuels Including the Effects of Irradiation, ORNL/TM-2000/351*; Fissile Materials Disposition Program, Oak Ridge National Laboratory: Oak Ridge, TN, USA, 2000.
- [12] Wang, B. T.; Zheng, J. J.; Qu, X.; Li, W. D.; Zhang, P. *J. Alloy Compd.* **2015**, 628, 267-271.
- [13] Pelowitz, D. B.; Fallgren, A. J.; McMath, G. E. *MCNP6 User's Manual, Code Version 6.1.1beta, Manual Rev. 0, LA-CP-14-00745, Rev. 0*; Los Alamos National Security: Los Alamos, NM, USA, 2014.
- [14] Türkmen, M.; Sökmen, C. N. In *XI. Ulusal Nükleer Bilimler ve Teknolojileri Kongresi*, Kuşadası, Turkey, 12–14 October 2016, 2016 (in Turkish).